International Communication in Computational Mechanics

Journal homepage:
https://karyailham.com.my/index.php/iccm
ISSN: 3093-7205

Investigation of Mass Transfer in Generalized Power Law Blood Flow through Multiple Stenosed Artery

Kannigah Thirunanasambantham[1], Zuhaila Ismail[1,*], Lim Yeou Jiann[1], Amnani Shamjuddin[2] , Yahaya Shagaiya Daniel[3]

[1] Department of Mathematical Sciences, Faculty of Science, Universiti Teknologi Malaysia,81310, Johor Bahru, Malaysia
[2] Chemical Reaction Engineering Group (CREG), Faculty of Chemical and Energy Engineering, Universiti Teknologi Malaysia, 81310, Johor Bahru, Malaysia
[3] Department of Mathematical Sciences, Faculty of Science, Kaduna State University, Nigeria

ARTICLE INFO

Article history:
Received 8 November 2024
Received in revised form 21 November 2024
Accepted 9 December 2024
Available online 15 March 2025

Keywords:
Mass transfer; multiple stenosis; generalized power law; COMSOL multiphysics

ABSTRACT

Multiple stenosis refers to the deposition of plaque in an arterial lumen resulting from the development of atherosclerosis. In the presence of stenosis, the arterial wall narrows, thereby limiting blood flow and nutrient delivery to other organs and tissues. This study investigates mass transfer in a generalised power-law blood flow through an artery with multiple stenoses. COMSOL Multiphysics is used to simulate and analyse the mass transfer and blood flow through the stenosed artery. The results demonstrate that the severity of stenosis alters blood flow and mass concentration in the blood. The diffusion rate decreases at the stenotic region as the severity increases. The study demonstrates a twice increase in velocity and mass accumulation at the stenotic region. Findings show that the distance between multiple stenoses significantly impacts the formation of the recirculation zone. The mass concentration rises, and the diffusion flux reduces significantly. These insights provide guidance for optimising drug delivery through stenosed arteries, making it possible to develop advanced treatments for diseases associated with stenosis.

1. Introduction

Atherosclerosis specifically refers to plaque build-up in the arteries [1]. The plaques will restrict the blood flow and diminish oxygen supply to other parts of organs, reducing oxygen supply to those organs. Stenosis is caused by the accumulation of plaques and the narrowing of the arteries. The narrowing of the artery can potentially affect the artery's inner wall, known as the endothelium. The damage of the endothelium enables the accumulation of cholesterol, fats, and other substances along the arterial wall. Hence, this leads to restricting blood flow to other body organs as the stenosis progresses. Eventually, these further damages and increases the inflammation in the wall of the artery, exacerbating plaque build-up. These may cause chest pain (angina), heart attack, stroke,

* *Corresponding author.*
E-mail address: zuhaila@utm.my

https://doi.org/10.37934/iccm.1.1.5274

extreme fatigue, shortness of breath, or, worst case, heart failure [2]. Invasive coronary angiography is currently considered the best method for evaluating the extent of atherosclerosis. However, it has some limitations, such as the 2-dimensional nature of the images produced, which can vary depending on the projection angle, according to a study by Saveljic *et al.,* [3]. This can lead to potential inaccuracies in the visual assessment of stenoses during angiography and make it difficult to determine the functional significance of the lesions accurately. Additionally, the geometry of the arteries and the location of stenoses may play a crucial role in assessing the impact of hemodynamic on the formation of stenoses [4].

In terms of clinical illness, the four major arteries that display the highest prevalence of clinical illness are the left coronary artery, abdominal aorta, carotid bifurcation, and the heart and proximal aorta [5]. Fluid loading on the artery walls could change dramatically in arteries and arterioles with significant curvatures, especially at bifurcations and junctions. This is why atherosclerotic lesions develop more often at these locations [6]. In both experimental and theoretical studies, stenoses lead to arterial insufficiency symptoms. Studies showed that multiple stenoses with different severities can have a synergistic effect, leading to more severe symptoms and potentially an increased risk of complications. Dhange *et al*., [7] and Dolui *et al*., [8] investigated the impact of multiple stenoses on an artery to blood flow. The severity and distance between each stenosis in a multiple stenoses geometry affects the velocity and pressure of the blood flow in the artery [7]. The spacing between stenoses significantly affects blood flow and energy loss. Blood flow through numerous stenoses has also been studied by [9-11]; however, these investigations have not considered the mass transfer.

Mass transfer (delivery of nutrients) in arterial blood flow plays a significant role in atherosclerosis development [12]. Atherosclerosis lowers the oxygen level in stenosed arteries. Examining oxygen transport in arterial blood flow with stenoses is crucial. This concept of mass transport in arterial blood flow refers to the movement of oxygen and low-density lipoproteins from the circulating blood to the arterial walls and back again. Researchers have studied how atherosclerosis is linked to the movement of substances in the blood using different fluid flow models in narrowed arteries [13]–[16]. They found that the existence of the stenoses has significantly affected the mass transfer in the artery. Sarifuddin *et al.,* [17] analysed the progression of stenosis over a time period and found that the severity and location of stenosis impact blood flow and the transport of critical substances. The blood rheological model is another important aspect to consider in studying blood flow with stenosis. In addition, Zaman *et al.,* [36] studied heat and mass transfer on overlapping stenoses, concluding that the mass concentration increases with increasing stenotic height and the WSS decreases with increasing Weissenberg number. Mass transfer has not been taken into account in the majority of research investigations that have examined blood flow via numerous stenoses. In addition, clinically, interventions for arterial stenosis, such as angioplasty or stenting, are designed to restore normal blood flow. While mass transfer is important for long-term arterial health, immediate clinical concerns often focus on re-establishing adequate blood flow [18]. However, after interventions like stenting or angioplasty, the altered flow dynamics can affect mass transfer. Not considering this can lead to a lack of understanding of how these changes impact long-term outcomes and restenosis (re-narrowing of the artery) [19]. The arterial system's bifurcations, curves, and other places with complex blood flow patterns are often the sites of atherosclerotic accumulation [1]. Furthermore, vascular mass transport is believed to be influenced by biomechanical forces, specifically WSS. Additionally, according to Reddy *et al.,* [20], the reason for lipid build-up and hypoxia in the arterial wall is low WSS, as evidenced by the concentration of LDL and declining oxygen concentration in the subendothelial layer of the arterial wall where WSS is low. More research is required to take mass

transfer into account when mathematically simulating blood flow across the multiple stenosed artery.

It has been noted that blood in various diseased conditions possesses non-Newtonian characteristics [21]. Since blood viscosity varies with shear rate, blood behaviour is more accurate to be treated as a non-Newtonian model. Due to the clumping of red blood cells in low shear zones, big particles are produced (rouleaux). These rouleaux become more tightly packed and more likely to adhere to the endothelium. This leads to inflammation and, ultimately, atherosclerosis [22]. This phenomenon increases the viscosity of blood, highlighting its non-Newtonian behaviour. The condition typically occurs in smaller branches and capillaries downstream of the stenotic zone, particularly in damaged vessels [23]. Recent studies have been conducted using non-Newtonian models, including models: Generalised power law (GPL) [21,24-26], Carreau-Yasuda models [27-29], modified Casson models [16,30,31], Herschel-Bulkley models [32-34] and Cross models [35,36]. Ikbal *et al.,* [37] concluded that the GPL model is the most generic model for non-Newtonian models due to its unique characteristics as a Newtonian model at low shear rates, a power law model at high shear rates, as well as a Casson model in certain circumstances. Sabaruddin *et al.*, [2] agreed with Ikbal *et al.,* [37] on the use of a GPL model. The authors investigated various generalised classical models and found that the GPL model accurately approximates the wall shear stress (WSS) in a low-shear zone. High-risk plaques and blood clots can be accurately predicted if the WSS values can be forecasted accurately [38]. Additionally, the GPL model is better at predicting the WSS for low input velocities than the Newtonian model [39].

Taking into account the literature survey discussed above [1,15,40], the study of GPL blood flow through multiple stenoses arteries with mass transfer has not yet been performed based on the authors' knowledge. Specifically, this study examines blood flow characteristics and mass transfer in straight arteries with double stenoses. A recent scientific study used computational techniques and numerical solutions to examine blood flow, heat, and mass transport in the stenosed artery [12]. However, assessing mass transfer in the double stenosed artery with varying occlusion of stenoses has yet to be investigated. Analysing blood flow is vital because it plays a key role in the development of dangerous illnesses like heart attacks and strokes. More research is required to take mass transfer into account when mathematically simulating blood flow across the arterial system's multiple stenoses. Most patients initially dismiss the first occurrence of stenosis in an artery due to its subtle effects [41]. However, as time progresses, the stenosis tends to worsen, and the likelihood of a second stenosis forming increases, thereby significantly affecting blood flow characteristics [42]. This study examines the blood flow dynamics in cases of double stenosis, with varying severities and distances between successive stenoses, to determine the blood flow characteristics and identify the stage at which this condition poses a significant risk, which is a significant contribution to this study.

There is a need to further study by considering the manipulated variables in the artery aids in analysing the characteristics of blood and mass flow, which is essential in the case of drug delivery. This study develops a mathematical model based on the GPL fluid model to describe the rheology of blood. Manipulation of the severity of the stenoses and the distance between them is taken into account in the present research, which is significant in this study. It is proposed that the numerical simulation of arterial blood flow is carried out using a computational fluid dynamics (CFD) method as it constitutes the most accurate method for solving the complicated problem of mass transfer in arterial blood flow. Numerical simulations can provide detailed insights into the flow dynamics at any level that may be difficult to achieve experimentally. This includes visualising velocity profiles, pressure distributions, and shear stresses within the blood vessels. Simulations allow for a granular understanding of the fluid mechanics that may be challenging to capture with specific experimental techniques [22]. Furthermore, using CFD in simulating blood flow includes noninvasive analysis,

patient-specific simulations, flow visualisation, calculation of hemodynamic parameters, predictive capabilities, cost and time efficiency, optimisation and design opportunities, and sensitivity analysis [43]. Thus, the present study applies the computational numerical technique via the COMSOL Multiphysics, which was developed based on finite element methods (FEM), to simulate the mass transport and momentum of the GPL blood rheology through a rigid wall of double stenosed artery. The artery is assumed to be rigid as fats, such as cholesterol, accumulate and build up in the wall [44]. Solving the developed mathematical model is intended to contribute greatly to the solution of the arterial stenoses issue, thus increasing the medical field's understanding of how to deal with atherosclerosis. These benefits contribute to a better understanding of blood flow dynamics, aid in disease diagnosis and treatment planning, and improve the design and evaluation of medical interventions.

2. Mathematical Formulation

A two-dimensional axisymmetric, laminar, steady, incompressible GPL model is considered. Figure 1 represents the geometric representation of the problem, where the radius of the artery is denoted as a. δ_1 and δ_2 are the depth of the severity of the first and second stenosis, respectively, l_0 is the outlet segment, l_2 is the distance between the double stenosis, $l_1$and, l_3 are the lengths of stenoses and l_4 is the inlet segment.

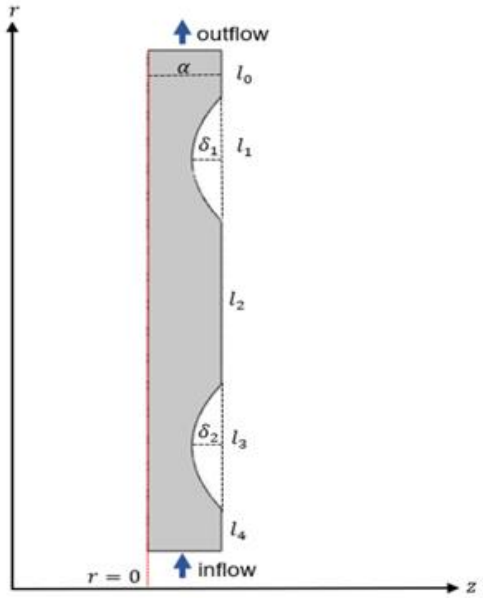

Fig. 1. Visual illustration of double stenoses in an artery

The equations governing flow in a cylindrical coordinates system can be stated in non-dimensional forms as follows [1]:

$$r\frac{\partial w}{\partial z}+\frac{\partial (ur)}{\partial r}=0, \tag{1}$$

$$\frac{\partial (wu)}{\partial r}+\frac{(\partial w^2)}{\partial z}+\frac{wu}{r}+\frac{\partial p}{\partial z}=-\frac{1}{\mathrm{Re}}\left[\frac{1}{r}\frac{\partial (r\tau_{rz})}{\partial r}+\frac{\partial (\tau_{zz})}{\partial z}\right], \tag{2}$$

$$\frac{\partial(wu)}{\partial z}+\frac{(\partial u^2)}{\partial r}+\frac{u^2}{r}+\frac{\partial p}{\partial r}=-\frac{1}{\mathrm{Re}}\left[\frac{1}{r}\frac{\partial(r\tau_{rr})}{\partial r}+\frac{\partial(\tau_{rz})}{\partial z}\right], \tag{3}$$

$$w\frac{\partial C}{\partial r}+u\frac{\partial C}{\partial z}=-\frac{1}{\mathrm{Re}\,Sc}\left[\frac{\partial^2 C}{\partial z^2}+\frac{1}{r}\frac{\partial C}{\partial r}+\frac{\partial^2 C}{\partial r^2}\right] \tag{4}$$

$$\text{where, } \mathrm{Re}=\frac{\rho R_0^n}{mU^{n-2}} \text{ and } \mathrm{Sc}=\frac{mR^{1-n}}{\rho D_m U^{1-n}} \tag{5}$$

$$\tau_{zz}=-2\left\{m\left|\left[\left(\frac{\partial u}{\partial r}\right)^2+\left(\frac{u}{r}\right)^2+\left(\frac{\partial w}{\partial z}\right)^2+\left(\frac{\partial u}{\partial z}+\frac{\partial w}{\partial r}\right)^2\right]^{\frac{1}{2}}\right|^{n-1}\right\}\times\left(\frac{\partial w}{\partial z}\right), \tag{6}$$

$$\tau_{rz}=-\left\{m\left|\left[\left(\frac{\partial u}{\partial r}\right)^2+\left(\frac{u}{r}\right)^2+\left(\frac{\partial w}{\partial z}\right)^2+\left(\frac{\partial u}{\partial z}+\frac{\partial w}{\partial r}\right)^2\right]^{\frac{1}{2}}\right|^{n-1}\right\}\left(\frac{\partial w}{\partial z}+\frac{\partial u}{\partial z}\right), \tag{7}$$

$$\tau_{rr}=-2\left\{m\left|\left[\left(\frac{\partial u}{\partial r}\right)^2+\left(\frac{u}{r}\right)^2+\left(\frac{\partial w}{\partial z}\right)^2+\left(\frac{\partial u}{\partial z}+\frac{\partial w}{\partial r}\right)^2\right]^{\frac{1}{2}}\right|^{n-1}\right\}\times\left(\frac{\partial u}{\partial r}\right). \tag{8}$$

The parameters *u* and *w* denote radial and axial velocity components in r and z direction in the spherical coordinates, respectively. The mass concentration is specified as C, and the radius of the artery is denoted as R_o. The dimensionless parameter, such as Re, is the Reynolds number, and Sc is the Schmidt number, expressed in Eq. (5). In addition, the component U is the flow speed and the diffusivity component in the blood is expressed as D_m. Parameter *m* is the consistency index, and *n* is the power index of the GPL model. Following that, the stress tensor is denoted as τ , the blood density is denoted as *ρ* and pressure is expressed as *p*. It is assumed that the arterial wall is rigid. Therefore, the bloodstream's velocity boundary conditions are the standard no-slip conditions [45], where $r = R(z)$ is the radius of the arterial segment in the stenotic region.

$$u(r,z)=v(r,z)=w(r,z)=0 \text{ on } r=R(z)$$

It is assumed that the radial and micro-rotational fluid flows parallel to the axis, as well as the axial velocity gradient, are zero, which can be expressed mathematically as follows:

$$v(r,z)=0, w(r,z)=0, \frac{\partial u(r,z)}{\partial r}=0, \text{on } r=0$$

A fully developed parabolic velocity corresponding to Hagen-Poiseuille [1] is assumed to occur initially when the system is at rest. In order to induce the parabolic velocity profile inlet [45], the following conditions are required:

at $z=0;\quad u\left(r,0\right)=0,$ and $w(r,0)=u\_\max\left(1-\left(\frac{r}{a}\right)^2\right)$ (parabolic inlet)

At the outlet, traction-free conditions are applied [45], which can be described as follows:

$$\left(-p\mathbf{I}+\tau\right)\mathbf{n}=0.$$

It is denoted by **n** that an outward normal vector with a pressure point constraint is defined p=0, and **I** is the unit tensor. It is proposed that mass concentration axial symmetry conditions [1] are as follows:

$$\frac{\partial C\left(r,z\right)}{\partial r}=0 \text{ on } r=0.$$

The mass concentration of the solute is considered to be constant at the input, whereas the concentration gradient is zero at the outflow of the finite-length artery *L*, which can be expressed non-dimensionally as [1]:

$$C\left(r,z\right)=1 \text{ at } z=0 \text{ and } \frac{\partial C\left(r,z\right)}{\partial r}=0 \text{ at } z=L.$$

A Dirichlet boundary condition with zero concentration on the artery wall can be described as follows Reima *et al.,* [1]:

$$C\left(r,z\right)=0 \text{ on } r=R\left(z\right),$$

As a result, the relationship between mass transport in the blood and mass transfer inside the artery wall is essentially ignored. It is fair to assume no concentration on the wall when the fluid-side mass transfer resistance is greater than the wall-side resistance, as demonstrated by Reima *et al.,* [1]. Exceptionally, at the inlet, where the initial mass concentration of the solute is zero,

$$C\left(r,z\right)=0 \text{ for } z>0.$$

In this study, the governing equations for mass transport simulations in an artery with multiple stenoses were solved by utilising the COMSOL Multiphysics software. Using COMSOL Multiphysics' built-in CAD tools, a two-dimensional axisymmetry artery was constructed. The geometry used in this study is idealised; however, patient, patient-specific geometry needed to be used in order to simulate more accurate results. Nevertheless, to simplify the complexity of the study and also to understand the behaviour of blood flow with mass transport in different severity of stenoses, idealised geometry based on Reima *et al.,* [1] is applied. The numerical results presented in this section have been

obtained using a mesh that has been constructed with extra fine element sizes. Two physics models, Laminar Flow and Transport of Diluted Species, were used to calculate the velocity, mass concentration, and WSS of different severities of stenosis in COMSOL Multiphysics. In addition to examining the area occlusion, multiple stenoses are also examined in terms of distance. The characteristics of blood and mass transport were also analysed by varying the severity of the occlusion area and the distance between the stenoses, as shown in Tables 1 and 2. Using the parameters from Reima *et al.,* [1], Reynold's number of Re= 250 and Schmidt's number of Sc= 3000 were applied.

Table 1
The severity of stenoses with constant distance between two stenoses (l_2= 1)

Severity of area of occlusion	δ_1	δ_2
Case 1	0.2	0.6
Case 2	0.4	0.2
Case 3	0.6	0.3

Table 2
The distance between two stenoses at a constant severity (δ_1=0.6, δ_2 = 0.3)

Distance between two stenoses	l_2
Type 1	0.9
Type 2	0.7
Type 3	0.5

3. Validation and Mesh Test

In order to ensure mesh parameters did not negatively impact the findings, this study made several efforts at mesh refining. This study also computes the maximum velocity and number of domain elements using COMSOL Multiphysics, as shown in Table 3. The mesh test aims to demonstrate that results are independent of the number of elements. Figure 2 illustrates the saturation of mesh with varying element sizes.

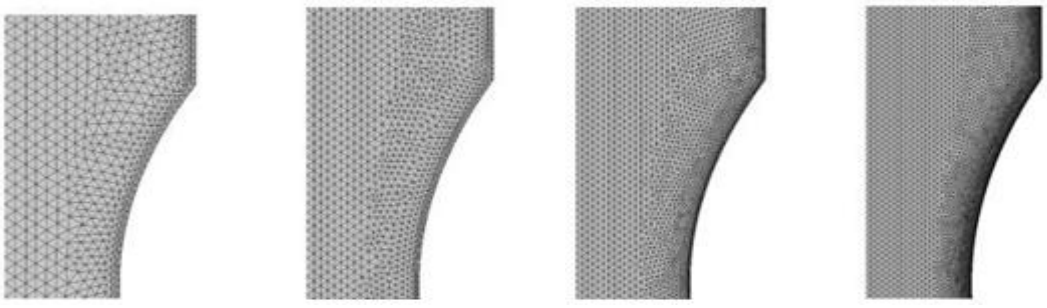

(a) (b) (c) (d)

Fig. 2. Mesh with various element sizes with partially magnified section. (a) mesh 1, normal element size. (b)mesh 2, fine element size (c) mesh 3 with a finer element size. (d) mesh 4, extra fine element size.

Based on Table 3, we can see that the maximum velocity obtained from the meshing of all sizes of domain elements is nearly the same. This justifies the independence of the meshing; hence, the

Mesh 4 with extra fine element size is utilised to mesh the geometry to achieve accuracy, consequently aiding in getting a better result.

Table 3
Results of mesh parameter in 2D axisymmetric model

	Mesh 1	Mesh 2	Mesh 3	Mesh 4
Domain Elements	5760	11354	24084	52502
Maximum velocity (m/s)	2.91845	2.93016	2.93320	2.93326

The model was validated by comparing the two-dimensional model developed in this study with the benchmark fluid problem in Ghia *et al.,* [46]. As part of the validation process, the lid-driven cavity will be used as a benchmark for evaluating numerical methods as well as fluid characteristics and behaviour in confined volumes with incompressible flows driven by the tangential motion of a bounding wall [46]. Figure 3 illustrates the streamline of the velocity plot. In Figure 3, the velocity streamlines are in excellent accord with Ghia *et al.,* [46] for every Reynolds number, Re=100, 400, and 1000.

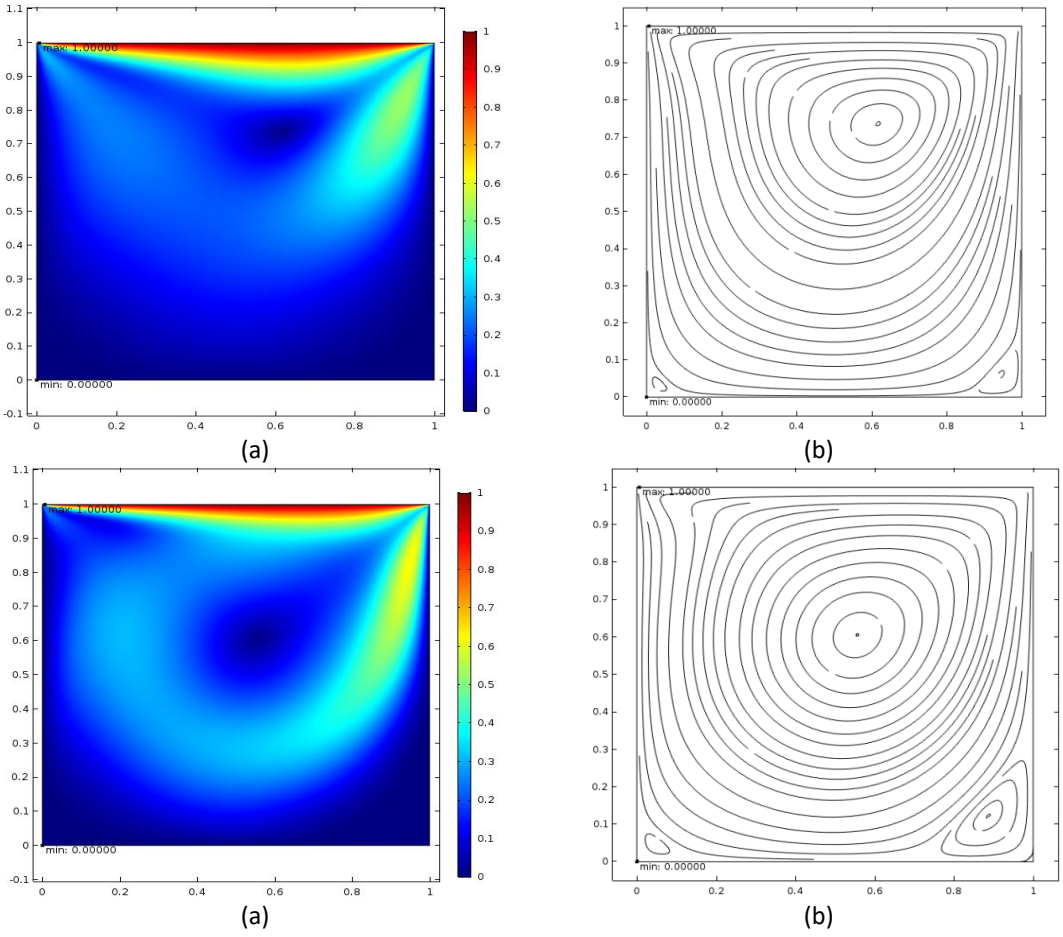

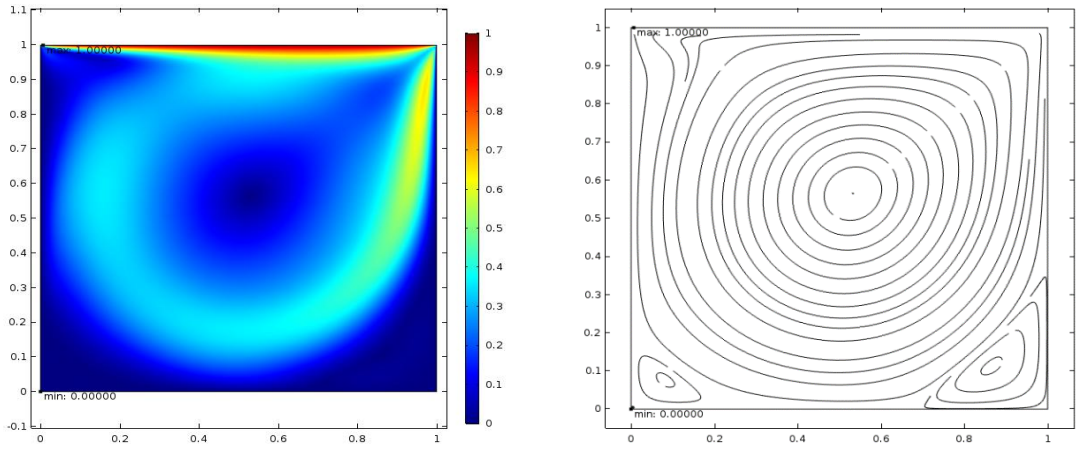

(a) (b)

Fig. 3. Velocity contour and streamline for lid-driven cavity problem with (a) Re=100, (b) Re=400, and (c) Re=1000

Credible Re parameters are used to determine the significance of model validation. A comparison is also made between the axial and radial velocities of the cavity at coordinate (0.5, 0.5), as shown in Tables 4 and 5. As seen from the comparison of Tables 4 and 5, the present result is nearly identical to that of Ghia *et al.,* [46], where fine-mesh solutions exhibit greater counter-rotating vortices as Re rises. Initially, vortices appear near the corners or the walls, but as Re increases, their centres slowly move towards the cavity centre. As a result, the velocity and vortex contours produced by this study's source code were the same as those acquired by Ghia *et al.,* [46], as seen in Figure 3. The numerical validation demonstrated the applicability of the developed techniques. Due to its reliability, it overcame the challenges inherent in this current investigation, which are discussed in further detail in the following section.

Table 4
Vertical line *u*-velocity through cavity geometric center

Re	Current Study	Ghia *et al.,* [46]
100	-0.20488	-0.20581
400	-0.11351	-0.11477
1000	-0.05958	-0.06080

Table 5
Horizontal line *v*-velocity through cavity geometric center

Re	Current Study	Ghia *et al.,* [46]
100	0.05691	0.05454
400	0.05384	0.05186
1000	0.02653	0.02526

4. Results and Discussion

Figure 4 illustrates the velocity streamline, magnitude and velocity surface results obtained from the simulation study. The parameters, such as the severity of stenoses and the distance between each stenosis, are set as $(\delta_1 = \delta_2 = 0.4)$ and $l_2 = 1$, respectively, based on Reima *et al.,* [13]. Figure 4(a) illustrates the presence of flow recirculation in the flow field of the non-Newtonian fluid flowing through a fully developed narrow artery. This raises the risk of atherosclerosis yet again. The

velocity in double stenoses is observed to have two major peaks. Based on contour plots shown in Figure 4, the velocity profiles extend gradually and smoothly downstream of the stenosis. As shown in Figure 4(a), the flow in the stenosis model experiences a small and weak recirculation zone. At the throat of stenosed arteries, distinct velocities with rapid changes in magnitude are also observed.

Figure 5 illustrates the axial velocity profile at the location of the evaluation L_1 (*r=0.5, z=3.75*) for different power-law indices, *n*. The velocity is observed to be higher with an increasing value of *n* at the inlet. However, as the fluid flows, the velocity decreases with increasing value of GPL index *n*. Generally, maximum velocity is predicted by the shear-thinning model (*n =0.639*), and minimum velocity is observed in the shear-thickening model (*n =1.2*) [14]. As a result, it is possible that the shear-thinning fluid flows faster and has a greater momentum due to changes in the apparent viscosity of fluids due to different generalised power laws indexes *n*. Power Law models exhibit a decreasing viscosity as the shear rate increases, consistent with the shear-thinning phenomenon [39]. Meanwhile, the shear-thickening rheological behaviour is attained as the highest viscosity in the significant shear rate ranges.

The maximum velocity magnitude is similar in Case 1, which is at the highest compared to Case 2 and Case 3, as shown in Figures 6(a) and 6(c). Notably, the axial velocity of normal and stenosed arteries differs significantly. It is evident from the results that there is a sudden change in velocity peaks, and the velocity increases at the stenosis region. When the area of reduction of the stenosis is reduced, and the area of reduction in another stenosis suddenly increases, the velocity changes abruptly. In Figure 6(a), the velocity is very high at the outlet due to sudden occlusion at the end of the artery, which enhances the flow rate. In Figure 6(c), the occlusion occurs at the inlet of the artery; hence, the velocity increases and can return to the normal state as it flows towards the outlet. However, in Figure 6(b), Case 2, the maximum velocity is lower, and an increase in velocity has occurred throughout the artery. This is due to the severity of the occlusion area in both stenosis, which inhibits the velocity from returning to a normal state. As the area reduction increases, the axial velocity of the stenosis region increases. A twisting effect is created on the blood flow due to the velocity. It can be seen from Figure 6 that the intensity of the twisting effects increases as the blood flows downstream. A quantitative analysis comparing each severity case with Figure 4, where the occlusion is kept constant, showed a drastic increase in velocity of 180% when occlusion is worsened near the outlet of an artery. Nevertheless, the velocity percentile reduced to 104% when the severe occlusion formed further from the outlet of the artery. Consequently, an increase of 180% in velocity causes a nonlinear increase in the pressure drop across the stenosed portion. This potentially worsens the blockage and impedes blood flow, raising the risk of acute cardiovascular events such as heart attack or strokes, which is similar to the numerical research by Kaazempur *et al.,* [47]

The velocity at different positions of stenoses is also observed in Figure 7. The area reduction of stenoses is fixed at ($\delta_1 = 0.2$, $\delta_2 = 0.6$); however, the distance between the stenoses is reduced from $l_2 = 1$ to $l_2 = 0.9$,0.7 and 0.5, as stated in Table 1. The velocity profiles in all three positions are almost similar; however, the maximum velocity value increases as the distance between the two stenoses reduces. It can also be observed from the velocity streamlines that the intensity of blood flow increases as the stenoses are closer. Analytically, the velocity percentile across the artery rises to 0.12% when stenoses are close to each other. Conversely, a 0.05% increase in velocity is shown when the stenosis is further from each other. The velocity differences between each type are small because the flow is mainly impacted locally by the severity of stenosis [48]. The significance of the distance between two stenoses is lessened since the effect of a single severed stenosis on velocity is mostly limited to its immediate surroundings. Comparatively, our findings of velocity are consistent with Alsemiry *et al.,* [1].

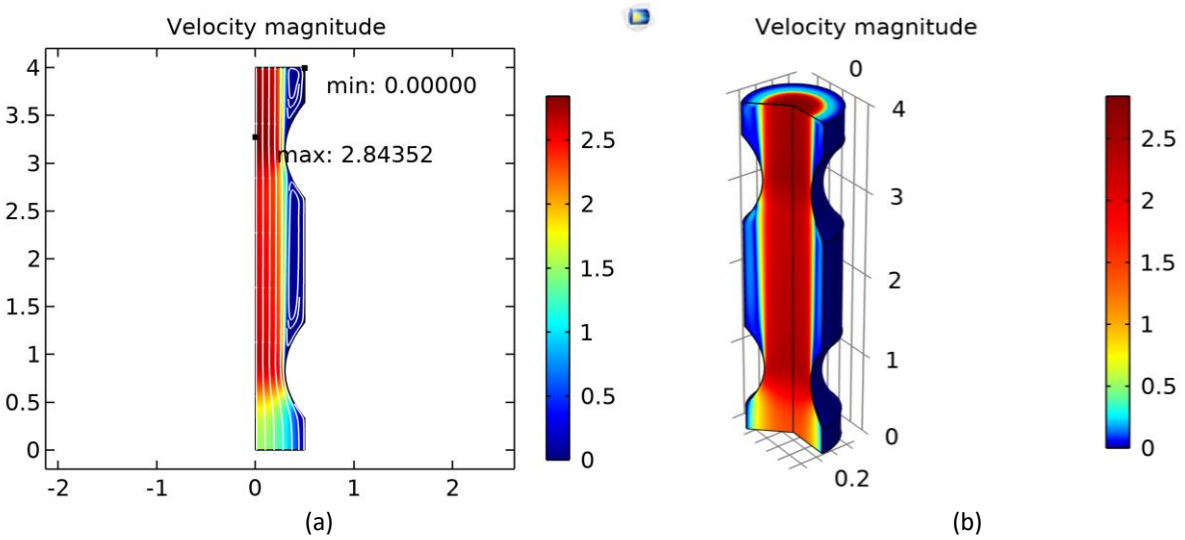

Fig. 4. Velocity magnitude and streamlines for the GPL model in (a) 2D axisymmetric and (b) 3D stenosed artery

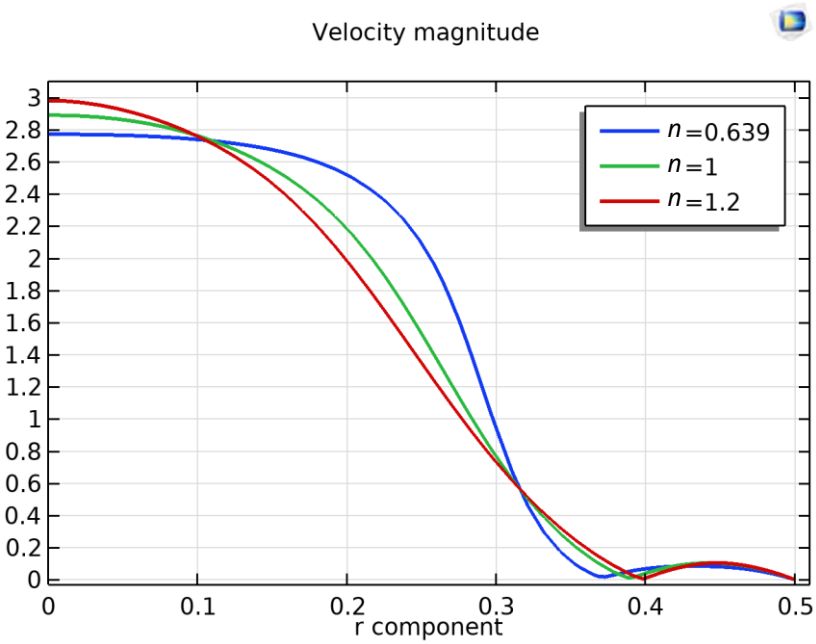

Fig. 5. Comparison of velocity profile with different power law values *n* =0.639, *n* =1 (Newtonian) and *n* =1.2 at location L_1 (*r=0.5, z=3.75*)

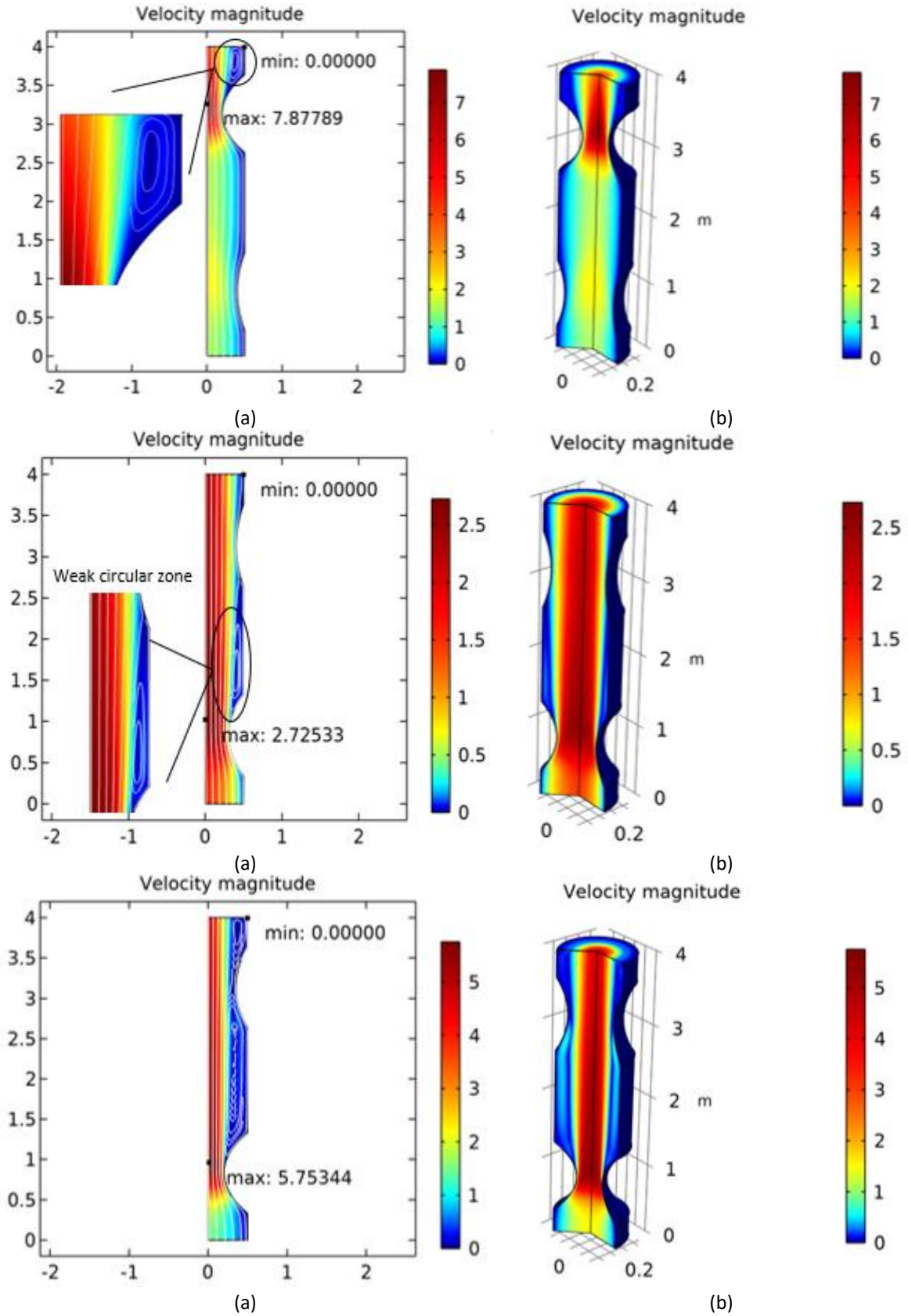

Fig. 6. Velocity magnitude and streamlines for the GPL model in 2D axisymmetric and 3D with different severities of area reduction of stenoses (a) Case 1, (b) Case 2 and (c) Case 3

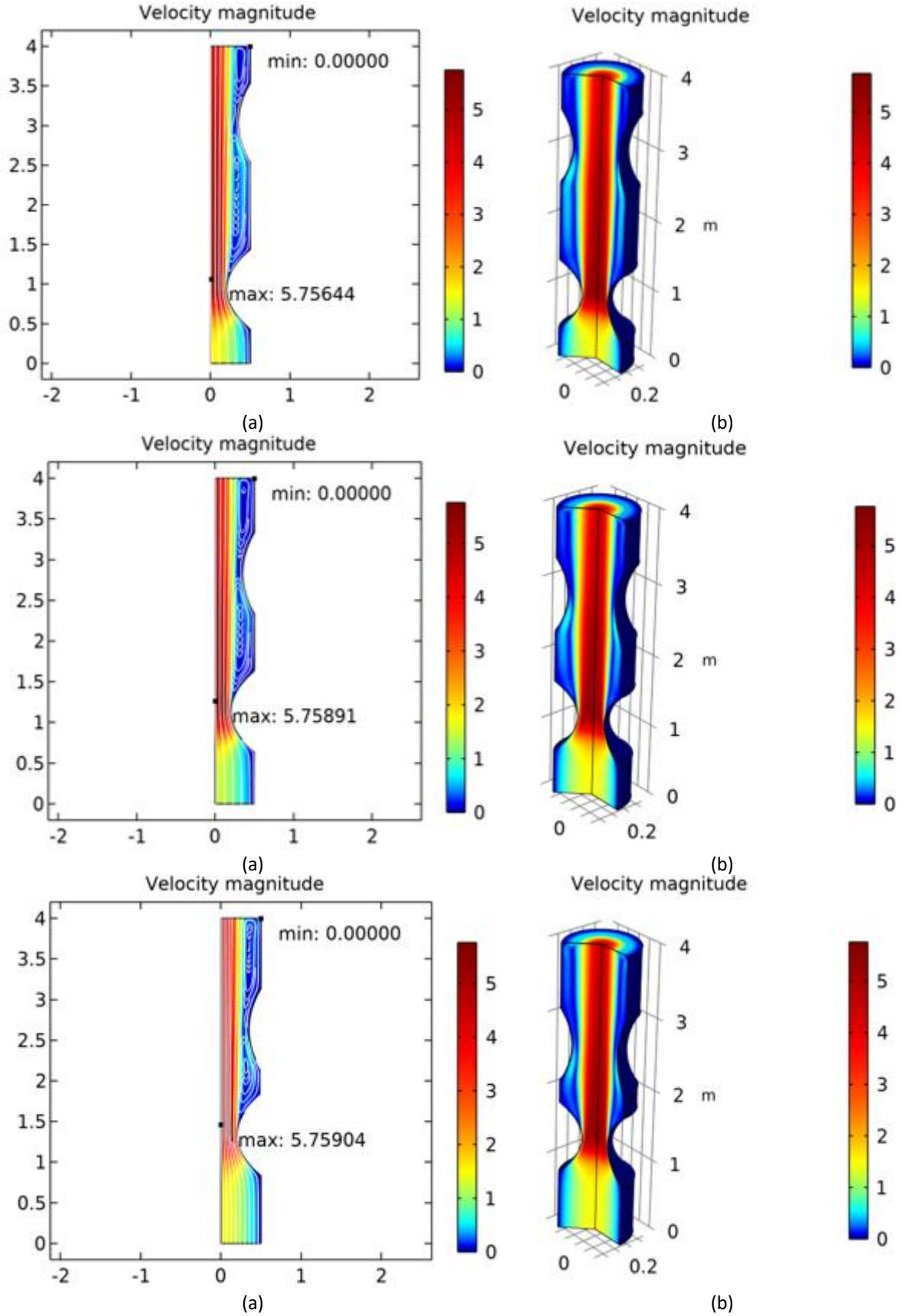

Fig. 7. Velocity magnitude and streamlines for the GPL model in 2D axisymmetric and 3D with different distances between the double stenoses (a) Type 1, (b) Type 2 and (c) Type 3

Figure 8 illustrates the surface contour for concentration, *C* transportation throughout the stenosed artery. Based on the two-dimensional and three-dimensional surface contour plots visualised in Figure 8, the concentration pattern follows the flow field for better understanding. Figure 8(a) shows that the concentration is disrupted towards the throat of the stenoses; along the first stenosis (bottom stenosis), concentration is low throughout the artery; however, at the stenosis region, the mass concentration increases. Higher mass transfer occurs at the second stenosis (upper stenosis) as the region possesses low flow velocity due to the separation of flow at the upper stenoses towards the outlet, which identifies a weak recirculation zone.

Figures 9 and 10 exhibit the line graph of mass concentration and diffusive flux comparison for all three cases at different stenosis severity, as stated in Table 4. It is observed from Figure 9 that the area of occlusion and velocity affect the solute concentration. From Case 1 ($\delta_1 = 0.2$ and $\delta_2 = 0.6$), the occlusion area at the outlet (top stenosis) is more severe than the other, resulting in a drastic increase in mass concentration due to the narrowness of the artery. The mass concentration is low at the centre of the artery and increases towards the stenosed region. Based on Case 1, the mass concentration is higher than in other cases due to severe occlusion at the outlet, increasing the mass accumulation across the artery. On the other hand, in Case 3 ($\delta_1 = 0.6$, and $\delta_2 = 0.3$), the area of occlusions is more severe at the inlet of the artery (bottom stenosis) than the other stenosis. Therefore, the mass concentration attained here is lower than in Case 1 in the stenosed region; however, towards stenosis, it increases gradually. Whereas in Case 2 ($\delta_1 = 0.4$ and $\delta_2 = 0.2$), the trend of mass concentration is constant and increases toward the artery wall as the occlusion area on both of the stenosis is not severely obstructed. In all cases, the mass concentration accumulated at the stenosed artery's wall. The mass concentration increased 8-12% at the post-stenotic region in Cases 1 and 3. Consequently, there is a low and stagnant velocity at the post-stenotic region of the artery, resulting in an increase in mass concentration towards the wall [47]. Overall, stenosis or narrowing of the artery changes mass concentration depending on velocity distribution.

Based on Figure 10, the diffusive flux rate in Case 1 ($\delta_1 = 0.2$ and $\delta_2 = 0.6$), the trendline starts at a high value and fluctuates towards the wall. In addition, a sudden fluctuation is seen at the stenosed region, followed by a slight increase before reducing to zero at the artery wall. This is due to the area of occlusion that is deeper at the outlet of the artery, which forces the diffusion flux to be higher, and a sudden drop is seen as it flows toward the stenosed region. The trendline of Case 3 is similar to Case 1 due to severe occlusion at the inlet; hence, the rate of mass transfer rate is higher in the beginning and decresase towards the wall. However, in Case 2 ($\delta_1 = 0.4$ and $\delta_2 = 0.2$), the mass transfer rate is lower than the one observed in Case 1 and Case 3 due to the low severity of stenosis. Hence, the rate of mass transfer in Case 2 is not entirely hindered by the mass of the solute from flowing through. However, unlike Case 1 and Case 3, in Case 2, the trendline reduces smoothly towards the stenosis wall, and the diffusive flux is distributed across the artery. Based on Case 1 and Case 3, the rate of mass transfer increases, and it fluctuates towards the narrow wall due to an increase in stenosis height near the outlet. At the stenosed region, the diffusive flux reduces to over -72%, proving the accumulation of mass accumulation is at the occlusion region in Case 1 and Case 3. Consequently, reduced diffusive flow in a stenosed area can greatly impact tissue health and function because vital substances are not adequately supplied and removed [27]. On the other hand, the diffusive flux for Case 2 is reduced to only 76% when the stenosis is not severe; therefore, the rate of mass transfer is still efficient.

Figure 11 depicts the profile of mass concentration at different positions of stenosis. The distance between the stenoses is observed to affect the mass concentration and fluid flow. Based on Figure 11, due to the severity of the top stenoses (near the outlet), the mass concentration for Type 3 (l_2=0.5) is discovered to increase higher at the stenotic region and then drastic increase to one at the

wall of the stenosis than the mass concentration obtained for Type 1 and Type 2. This is due to the shorter gap between each stenosis, hence the higher accumulation of the mass concentration. The mass accumulation of Type 3 (l_2=0.5) increased to 5% from Case 3 (l_2=1) in Figure 9. On the other hand, the mass concentration for Type 1 (l_2=0.9) increased slightly by 0.04%, and Type 2 (l_2=0.7) increased by 4.2% from Case 3 (l_2=1). As the distance between each stenosis decreases, the recirculation of flux at the post-stenotic region increases, resulting in an increased accumulation of mass concentration.

Figure 12 demonstrates the diffusive flux magnitude profile at different stenosis positions. It is observed that Type 1 (l_2=0.9) has a lower diffusion rate; however, the trendline has a quicker and smoother enhancement after the stenotic region, and then the diffusion rate fluctuates towards the wall. This occurs due to the distance of stenosis, which is further away from each other, and the increment of stenosis severity close to the arterial outlet. However, the diffusive flux for Type 2 (l_2=0.7) and Type 3 (l_2=0.5) have a higher diffusion rate and decrease drastically across the artery as the distance between each stenosis becomes closer. The diffusion rate fluctuates up to -88% when the distance between each stenosis is closer to each other, leading to further build-up of substances, eventually increasing the occlusion area of stenosis.

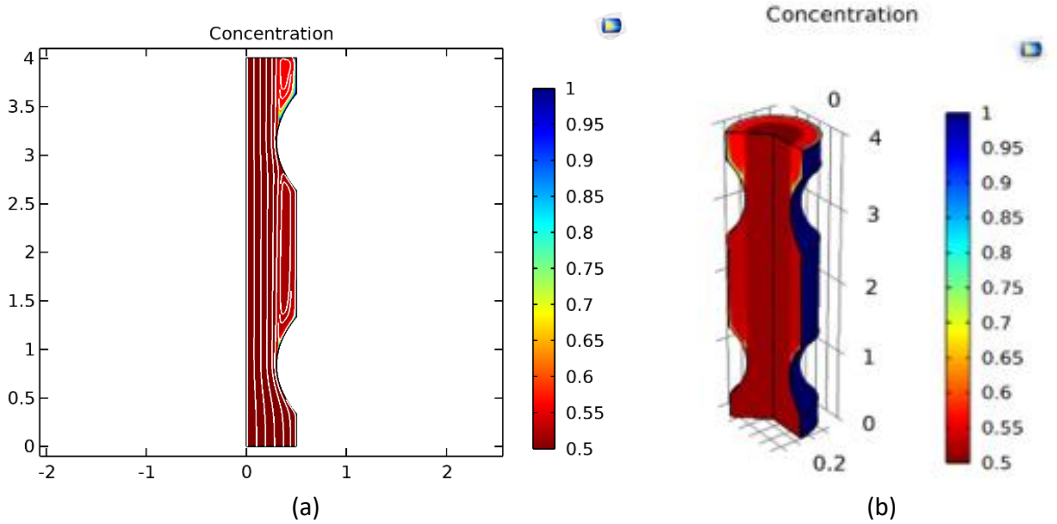

Fig. 8. Mass concentration of the GPL model (a) 2D axisymmetric and (b) 3D stenosed artery

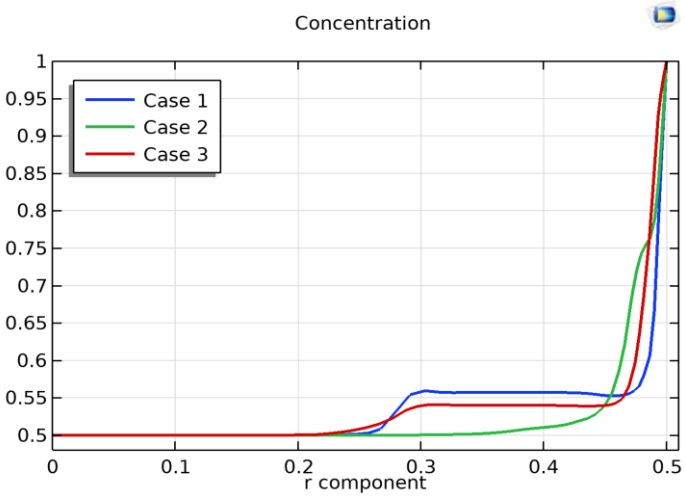

Fig. 9. Line graph of mass concentration of different severities of stenoses

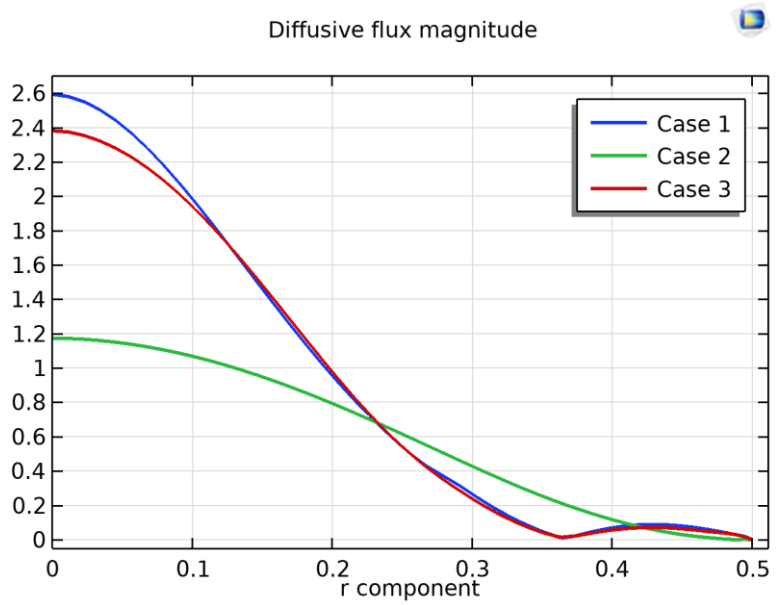

Fig. 10. Line graph of diffusive flux magnitude of different severities of stenoses.

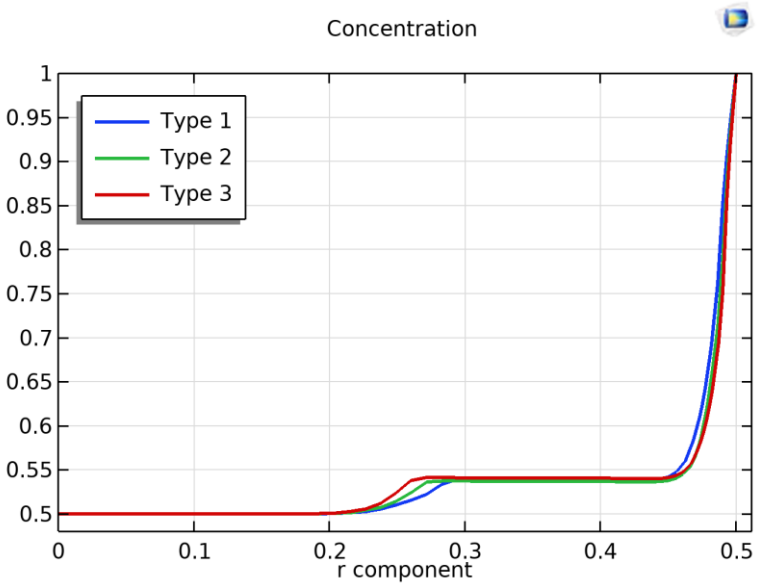

Fig. 11. Line graph of mass concentration of different distances between the double stenoses

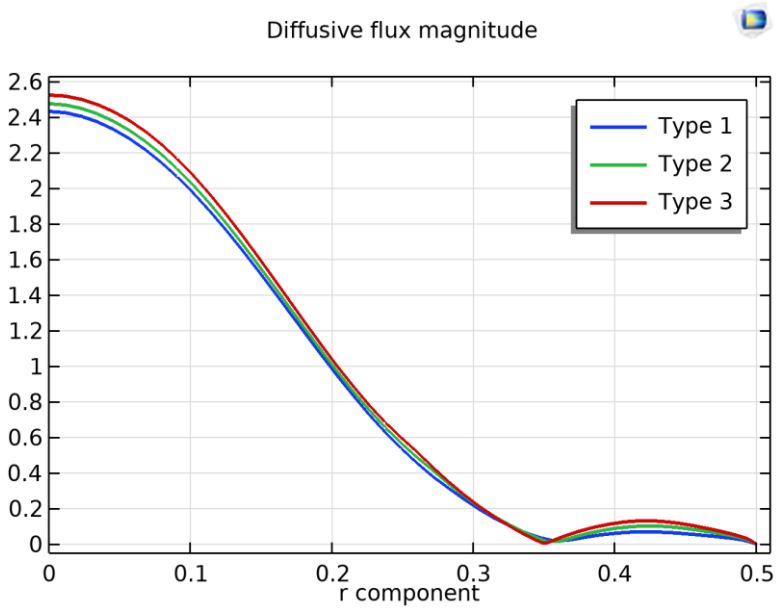

Fig. 12. Line graph of diffusive flux magnitude of the different distances between the double stenoses

WSS has been found to play an important part in investigating atherosclerosis in arteries [9]. Higher WSS values can result in plaque rupture. Plaque formation can also be attributed to low and oscillating WSS [44]. The wall of the artery with stenoses is analysed for WSS. In an artery without stenosis, the WSS exhibits a constant trendline. Plaque rupture can occur at this point due to the maximum WSS upstream from the throat. This is in agreement with the outputs of [23], [49]. From Figure 13, the WSS is observed to increase with an increase in the *n* value. With the increment in shear rate values, the viscosity of blood is increased; therefore, the non-Newtonian model (*n =1.2*), which acts according to the shear-thickening nature, exhibits the highest WSS, while the non-Newtonian model (*n =0.639*) that acts as shear-thinning fluid possesses the lowest WSS among these three different fluid characterisations.

Figure 14 illustrates that as the occlusion of the stenosis narrows further, the WSS increases due to an increasing severity level to maintain the flow rate. It is obvious from this value that WSS is maximal when the first stenosis has a greater area of reduction than the subsequent stenosis. It is clear from the current results that the WSS increases as the stenosis deepens. Based on Figure 15, the stenosis distance also affects the WSS value. This can be clearly seen in Figure 15, where the distance between two peaks decreases as the distance between two stenoses reduces. This could lead to a higher risk of plaque rupture due to immediate and sudden increments of WSS values from one stenosis to another.

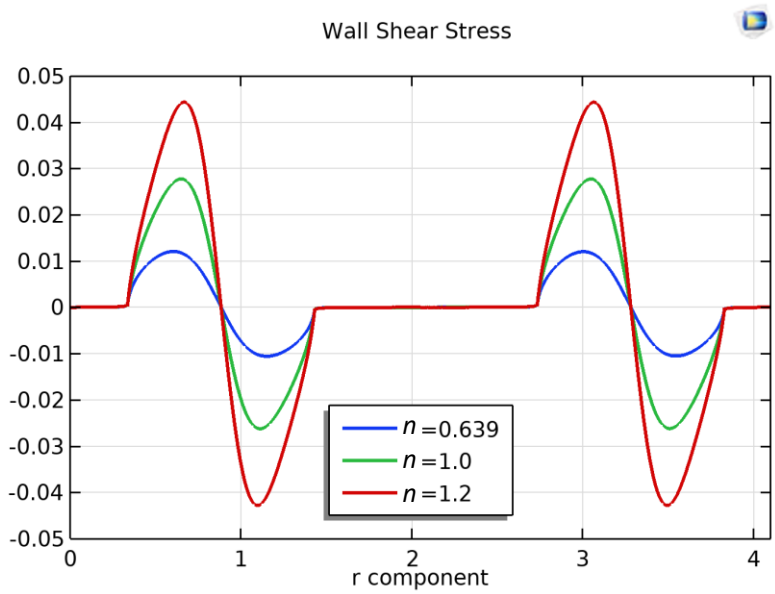

Fig. 13. Comparison of WSS with different power law value *n* =0.639, *n*=1(Newtonian), and *n* =1.2.

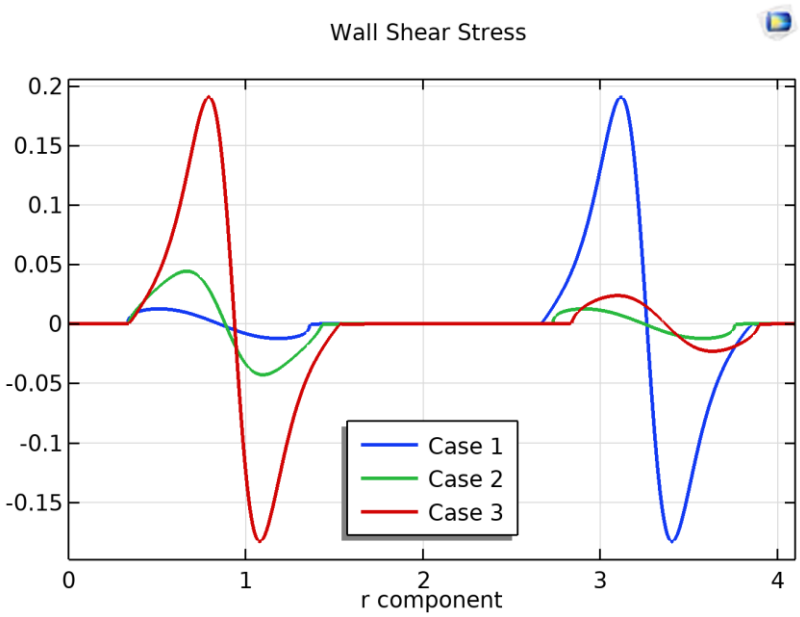

Fig. 14. WSS line graph for the GPL model of different severities of stenoses

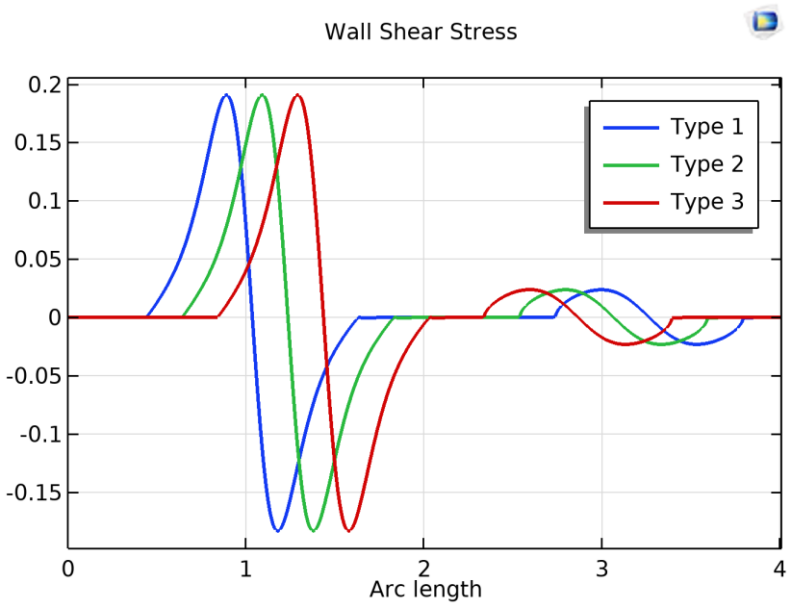

Fig. 15. WSS line graph for the GPL model of the different distances between the double stenoses

4. Conclusion

Atherosclerosis can be related to the nature of blood movement and the mechanical behaviour of blood vessels and arterial walls, so studying blood flow through a stenotic artery is crucial. Simulations are performed with double stenoses with different areas of reductions and distances between the stenoses. Each case is thoroughly examined and discussed graphically. As a result of the present numerical computations, below are the key conclusions obtained:

- A significant increase of 180% is seen in the velocity as the stenosis severity increases in each case; however, less than a percent velocity increase is shown as the distance between each stenosis reduces.
- As the reduction area increases, the velocity and mass concentration magnitudes increase. In proportion to the decrease in distance between successive stenoses, the maximum velocity and mass concentration also rise. It is evident that when there is a small distance between the two stenoses, the velocity streamline increases, causing difficulty in mass concentration flow.
- As the stenosis worsens, the diffusion flux decreases up to -72 %, causing flow stagnation and resisting the mass flow. In addition to the decrease in distance between successive stenoses, the diffusion flux further decreases up to -88%, causing a significant increase in mass accumulation.
- In the WSS simulation, the blood flow characteristics of the stenotic artery were also demonstrated. A high WSS in a stenotic region of the arterial rigid wall may indicate greater plaque disruption damage in atherosclerosis.

The findings from this study are based on the numerical simulation according to the boundary conditions applied. The findings shed light on the drastic behaviours of mass accumulation and velocity with different severity of stenosis. The results will be more accurate if patient-specific geometry is used in the study. In addition, the permeability of the wall and its effect on mass transfer can be considered in future work. In addition, by understanding the blood flow characteristics with mass transfer, effective drug delivery can be administered. This is because poor mass transfer can

result in inadequate drug distribution, reducing the treatment's effectiveness [50]. Moreover, insufficient oxygen transport (hypoxia) due to poor mass transfer can cause tissue damage and promote the progression of arterial diseases. This can exacerbate the condition and lead to complications such as ischemia [50]. Therefore, the provided information may be of value in understanding how mass transfer occurs in arterial blood flow, which might help in treating stenotic arteries and reducing the likelihood of restenosis after surgery. It is possible that our findings can be used to identify cardiovascular disease risk factors and find a solution to such diseases.

Acknowledgement
The current study is made possible by funding from Universiti Teknologi Malaysia (UTM), UTM Fundamental Research Vote No: Q.J130000.3854.23H57 and PAS Q.J130000.2754.04K09

References

[1] Alsemiry, Reima D., Sarifuddin, Prashanta K. Mandal, Hamed M. Sayed, and Norsarahaida Amin. "Numerical solution of blood flow and mass transport in an elastic tube with multiple stenoses." *BioMed research international* 2020, no. 1 (2020): 7609562. https://doi.org/10.1155/2020/7609562

[2] Jamali, Muhammad Sabaruddin Ahmad, and Zuhaila Ismail. "Generalized power law model of blood flow in a stenosed bifurcated artery." *Annals of Mathematical Modeling* 1, no. 2 (2021). https://doi.org/10.33292/amm.v1i2.6

[3] Saveljic, Igor, Tijana Djukic, Dalibor Nikolic, Smiljana Djorovic, and Nenad Filipovic. "Numerical simulation of fractional flow reserve in atherosclerotic coronary arteries." In *2021 IEEE 21st International Conference on Bioinformatics and Bioengineering (BIBE)*, pp. 1-4. IEEE, 2021. https://doi.org/10.1109/BIBE52308.2021.9635457

[4] Liu, Biyue, and Dalin Tang. "Influence of distal stenosis on blood flow through coronary serial stenoses: a numerical study." *International Journal of Computational Methods* 16, no. 03 (2019): 1842003. https://doi.org/10.1142/S0219876218420033

[5] Saufi, Ommar Mykael Mat, Nur Amani Hanis Binti Roseman, Ishkrizat Taib, Nurul Fitriah Nasir, Ahmad Mubarak Tajul Ariffin, Nor Adrian Nor Salim, Shahrul Azmir Osman, Nofrizal Idris Darlis, and Ali Kamil Kareem. "Flow Characteristics on Carotid Artery Bifurcation of Different Aneurysmal Morphology." *CFD Letters* 15, no. 2 (2023): 25-40. https://doi.org/10.37934/cfdl.15.2.2540

[6] Abd Aziz, Azyante Erma, Muhammad Sabaruddin Ahmad Jamali, and Zuhaila Ismail. "Numerical simulation of generalised power law blood flow model through different angles of stenosed bifurcated artery." *Journal of Mathematics and Computing Science (JMCS)* 7, no. 2 (2021): 1-14. https://doi.org/10.33292/amm.v1i2.6

[7] Dhange, Mallinath, Gurunath Sankad, and Umesh Bhujakkanavar. "Blood Flow with Multiple Stenoses in a Force Field." *Mathematical Modelling of Engineering Problems* 8, no. 4 (2021). https://doi.org/10.18280/mmep.080406

[8] Dolui, Soumini, Bivas Bhaumik, and Soumen De. "Combined effect of induced magnetic field and thermal radiation on ternary hybrid nanofluid flow through an inclined catheterized artery with multiple stenosis." *Chemical Physics Letters* 811 (2023): 140209. https://doi.org/10.1016/j.cplett.2022.140209

[9] Kabir, Md Alamgir, Md Ferdous Alam, and Md Ashraf Uddin. "Numerical simulation of pulsatile blood flow: a study with normal artery, and arteries with single and multiple stenosis. " *Journal of Engineering and Applied Science* 68 (2021): 1-15.https://doi.org/10.1186/s44147-021-00025-9

[10] Ramdan, Salman Aslam, Mohammad Rasidi Rasani, Thinesh Subramaniam, Ahmad Sobri Muda, Ahmad Fazli Abdul Aziz, Tuan Mohammad Yusoff Shah Tuan Ya, Hazim Moria, Mohd Faizal Mat Tahir, and Mohd Zaki Nuawi. "Blood flow acoustics in carotid artery." *Journal of Advanced Research in Fluid Mechanics and Thermal Sciences* 94, no. 1 (2022): 28-44. https://doi.org/10.37934/arfmts.94.1.2844

[11] Dubey, Ankita, B. Vasu, O. Anwar Bég, and R. S. R. Gorla. "Finite element computation of magneto-hemodynamic flow and heat transfer in a bifurcated artery with saccular aneurysm using the Carreau-Yasuda biorheological model." *Microvascular Research* 138 (2021): 104221. https://doi.org/10.1016/j.mvr.2021.104221

[12] Basit, Muhammad Abdul, Muhammad Imran, Ali Akgül, Murad Khan Hassani, and Abdullah Alhushaybari. "Mathematical analysis of heat and mass transfer efficiency of bioconvective Casson nanofluid flow through conical gap among the rotating surfaces under the influences of thermal radiation and activation energy." *Results in Physics* 63 (2024): 107863. https://doi.org/10.1016/j.rinp.2024.107863

[13] Alsemiry, Reima D., Prashanta K. Sarifuddin, Hamed M. Sayed, and Norsarahaida Amin. "Effects of pulsatility and double stenoses on power law model of blood flow and mass transport in vessel." *Journal of Heat and Mass Transfer* 19, no. 1 (2020): 97-128. https://doi.org/10.17654/HM019010097

[14] Zain, Norliza Mohd, Zuhaila Ismail, and Peter Johnston. "A Stabilized Finite Element Formulation of Non-Newtonian Fluid Model of Blood Flow in A Bifurcated Channel with Overlapping Stenosis." *Journal of Advanced Research in Fluid Mechanics and Thermal Sciences* 88, no. 1 (2021): 126-139. https://doi.org/10.37934/arfmts.88.1.126139

[15] Yadav, Pramod Kumar, and Nitisha Yadav. "Impact of heat and mass transfer on the magnetohydrodynamic two-phase flow of couple stress fluids through a porous walled curved channel using Homotopy Analysis Method." *Chaos, Solitons & Fractals* 183 (2024): 114961. https://doi.org/10.1016/j.chaos.2024.114961

[16] Vaddemani, Ramachandra Reddy, Sreedhar Ganta, and Raghunath Kodi. "Effects of hall current, activation energy and diffusion thermo of MHD Darcy-Forchheimer Casson nanofluid flow in the presence of Brownian motion and thermophoresis." *Journal of Advanced Research in Fluid Mechanics and Thermal Sciences* 105, no. 2 (2023): 129-145. https://doi.org/10.37934/arfmts.105.2.129145

[17] Sarifuddin. "CFD modelling of Casson fluid flow and mass transport through atherosclerotic vessels." *Differential Equations and Dynamical Systems* 30, no. 2 (2022): 253-269. https://doi.org/10.1007/s12591-020-00522-y

[18] Chiastra, Claudio, Francesco Iannaccone, Maik J. Grundeken, Frank JH Gijsen, Patrick Segers, Matthieu De Beule, Patrick W. Serruys, Joanna J. Wykrzykowska, Antonius FW van der Steen, and Jolanda J. Wentzel. "Coronary fractional flow reserve measurements of a stenosed side branch: a computational study investigating the influence of the bifurcation angle." *Biomedical engineering online* 15 (2016): 1-16. https://doi.org/10.1186/s12938-016-0211-0

[19] Carson, Jason M., Neeraj Kavan Chakshu, Igor Sazonov, and Perumal Nithiarasu. "Artificial intelligence approaches to predict coronary stenosis severity using non-invasive fractional flow reserve." *Proceedings of the Institution of Mechanical Engineers, Part H: Journal of Engineering in Medicine* 234, no. 11 (2020): 1337-1350. https://doi.org/10.1177/0954411920946526

[20] Majeed, Afraz Hussain, Rashid Mahmood, Hasan Shahzad, Amjad Ali Pasha, Z. A. Raizah, Hany A. Hosham, D. Siva Krishna Reddy, and Muhammad Bilal Hafeez. "Heat and mass transfer characteristics in MHD Casson fluid flow over a cylinder in a wavy channel: Higher-order FEM computations." *Case Studies in Thermal Engineering* 42 (2023): 102730. https://doi.org/10.1016/j.csite.2023.102730

[21] Zain, Norliza Mohd, and Zuhaila Ismail. "Dynamic Response of Heat Transfer in Magnetohydrodynamic Blood Flow Through a Porous Bifurcated Artery with Overlapping Stenosis." *Journal of Advanced Research in Fluid Mechanics and Thermal Sciences* 101, no. 1 (2023): 215-235. https://doi.org/10.37934/arfmts.101.1.215235

[22] Kumawat, Chandan, B. K. Sharma, Qasem M. Al-Mdallal, and Mohammad Rahimi-Gorji. "Entropy generation for MHD two phase blood flow through a curved permeable artery having variable viscosity with heat and mass transfer." *International Communications in Heat and Mass Transfer* 133 (2022): 105954. https://doi.org/10.1016/j.icheatmasstransfer.2022.105954

[23] Roy, Ashis Kumar, and O. Anwar Bég. "Asymptotic study of unsteady mass transfer through a rigid artery with multiple irregular stenoses." *Applied Mathematics and Computation* 410 (2021): 126485. https://doi.org/10.1016/j.amc.2021.126485

[24] Zain, Norliza Mohd, Zuhaila Ismail, and Peter Johnston. "Numerical analysis of blood flow behaviour in a constricted porous bifurcated artery under the influence of magnetic field." *CFD Letters* 15, no. 1 (2023): 39-58. https://doi.org/10.37934/cfdl.15.1.3958

[25] Kakavand, Keyvan, Naser Koosha, Kaveh Fathi, and Saman Aminian. "Numerical investigation of capture efficiency of carrier particles in a Y-shaped vessel considering particle-particle interaction and Non-Newtonian behavior." *Journal of Drug Delivery Science and Technology* 67 (2022): 102997. https://doi.org/10.1016/j.jddst.2021.102997

[26] Thirunanasambantham, Kannigah, Zuhaila Ismail, Lim Yeou Jiann, and Amnani Shamjuddin. "Numerical Computational of Blood Flow and Mass Transport in Stenosed Bifurcated Artery." *Journal of Advanced Research in Fluid Mechanics and Thermal Sciences* 110, no. 2 (2023): 79-94. https://doi.org/10.37934/arfmts.110.2.7994

[27] Bensilakhal, Sara, Redha Rebhi, Noureddine Hadidi, Giulio Lorenzini, Yacine Kerchiche, Younes Menni, Houari Ameur, and Hijaz Ahmad. "Bi-stability Study of Double Diffusive Convection Using the Carreau-Yasuda Model in a Shallow Horizontal Porous Layer Filled with a Non-Newtonian Fluid." *Journal of Advanced Research in Fluid Mechanics and Thermal Sciences* 101, no. 1 (2023): 137-159. https://doi.org/10.37934/arfmts.101.1.137159

[28] Vaidya, Hanumesh, Kerehalli Vinayaka Prasad, Rajashekhar Choudhari, Shivaraya Keriyappa, Manjunatha Gudekote, and Jyoti Shetty. "Partial slip effects on MHD peristaltic flow of Carreau-Yasuda fluid (CY) through a planner micro-channel." *Journal of Advanced Research in Fluid Mechanics and Thermal Sciences* 104, no. 2 (2023): 65-85. https://doi.org/10.37934/arfmts.104.2.6585

[29] Averweg, Solveigh, Alexander Schwarz, Carina Schwarz, and Jörg Schröder. "3D modeling of generalised Newtonian fluid flow with data assimilation using the least-squares finite element method." *Computer Methods in Applied Mechanics and Engineering* 392 (2022): 114668. https://doi.org/10.1016/j.cma.2022.114668

[30] Azmi, Wan Faezah Wan, Ahmad Qushairi Mohamad, Yeou Jiann Lim, and Sharidan Shafie. "Slip Velocity Effect on

Unsteady Free Convection Flow of Casson Fluid in a Vertical Cylinder." *CFD Letters* 15, no. 5 (2023): 29-41. https://doi.org/10.37934/cfdl.15.5.2941

[31] Zaperi, Nur Husna Amierah Mohd, Nurul Aini Jaafar, and Duraisamy Sambasivam Sankar. "Solute Dispersion in Casson Blood Flow through a Stenosed Artery with the Effect of Temperature and Electric Field." *Journal of Advanced Research in Experimental Fluid Mechanics and Heat Transfer* 17, no. 1 (2024): 14-34. https://doi.org/10.37934/arefmht.17.1.1434

[32] Beleyur, Veena Sreenivasa. "Exploring the Dynamic Behavior of a Tapered Stenosed Artery: An Investigation into Its Unsteady Model." *Journal of Advanced Research in Fluid Mechanics and Thermal Sciences* 121, no. 2 (2024): 48-64. https://doi.org/10.37934/arfmts.121.2.4864

[33] Jaafar, Nurul Aini, Siti NurulAifa Mohd ZainulAbidin, Zuhaila Ismail, and Ahmad Qushairi Mohamad. "Mathematical analysis of unsteady solute dispersion with chemical reaction through a stenosed artery." *Journal of Advanced Research in Fluid Mechanics and Thermal Sciences* 86, no. 2 (2021): 56-73. https://doi.org/10.37934/arfmts.86.2.5673

[34] Tiwari, Ashish, Pallav Dhanendrakumar Shah, and Satyendra Singh Chauhan. "Unsteady solute dispersion in two-fluid flowing through narrow tubes: A temperature-dependent viscosity approach." *International Journal of Thermal Sciences* 161 (2021): 106651. https://doi.org/10.1016/j.ijthermalsci.2020.106651

[35] Haghighi, Ahmad R., and Nikou Pirhadi. "A Numerical Study of Heat Transfer and Flow Characteristics of Pulsatile Blood Flow in a Tapered Artery with a Combination of Stenosis and Aneurysm." *International Journal of Heat & Technology* 37, no. 1 (2019). https://doi.org/10.18280/ijht.370102

[36] Zaman, A., N. Ali, O. Anwar Bég, and M. Sajid. "Heat and mass transfer to blood flowing through a tapered overlapping stenosed artery." *International Journal of Heat and Mass Transfer* 95 (2016): 1084-1095. https://doi.org/10.1016/j.ijheatmasstransfer.2015.12.073

[37] Ikbal, Md A., S. Chakravarty, Kelvin KL Wong, Jagannath Mazumdar, and Prashanta K. Mandal. "Unsteady response of non-Newtonian blood flow through a stenosed artery in magnetic field." *Journal of Computational and Applied Mathematics* 230, no. 1 (2009): 243-259. https://doi.org/10.1016/j.cam.2008.11.010

[38] Pignani, Alessio, Ivan Di Venuta, Andrea Boghi, and Fabio Gori. "Mass transfer and blood flow in a patient-specific three-dimensional Willis circle." *International Communications in Heat and Mass Transfer* 126 (2021): 105369. https://doi.org/10.1016/j.icheatmasstransfer.2021.105369

[39] Zain, Norliza Mohd, and Zuhaila Ismail. "Modelling of Newtonian blood flow through a bifurcated artery with the presence of an overlapping stenosis." *Malaysian Journal of Fundamental and Applied Sciences* 13, no. 2017 (2017): 304-309. https://doi.org/10.11113/mjfas.v13n4-1.866

[40] Elogail, M. A., and Kh S. Mekheimer. "Modulated viscosity-dependent parameters for MHD blood flow in microvessels containing oxytactic microorganisms and nanoparticles " *Symmetry* 12, no. 12 (2020): 2114. https://doi.org/10.3390/sym12122114

[41] Meredith, Thomas, David Roy, David Muller, and Mayooran Namasivayam. "A Clinician's Guide to the Changing Aortic Stenosis Landscape: Updates in Aortic Stenosis Diagnosis, Surveillance and Management." *Current Treatment Options in Cardiovascular Medicine* 25, no. 11 (2023): 675-688. https://doi.org/10.1007/s11936-023-01020-4

[42] Grimard, Brian H., Robert E. Safford, and Elizabeth L. Burns. "Aortic stenosis: diagnosis and treatment." *American family physician* 93, no. 5 (2016): 371-378.

[43] Ningappa, Abhilash Hebbandi, Suraj Patil, Gowrava Shenoy Belur, Augustine Benjamin Valerian Barboza, Nitesh Kumar, Raghuvir Pai Ballambat, Adi Azriff Basri, Shah Mohammed Abdul Khader, and Masaaki Tamagawa. "Influence of altered pressures on flow dynamics in carotid bifurcation system using numerical methods." *Journal of Advanced Research in Fluid Mechanics and Thermal Sciences* 97, no. 1 (2022): 47-61. https://doi.org/10.37934/arfmts.97.1.4761

[44] Jamali, Muhammad Sabaruddin Ahmad, Zuhaila Ismail, and Norsarahaida Saidina Amin. "Effect of different types of stenosis on generalised power law model of blood flow in a bifurcated artery." *Journal of Advanced Research in Fluid Mechanics and Thermal Sciences* 87, no. 3 (2021): 172-183. https://doi.org/10.37934/arfmts.87.3.172183

[45] Jamali, Muhammad Sabaruddin Ahmad, and Zuhaila Ismail. "Simulation of Heat Transfer on blood flow through a stenosed bifurcated artery." *Journal of Advanced Research in Fluid Mechanics and Thermal Sciences* 60, no. 2 (2019): 310-323.

[46] Ghia, U. K. N. G., Kirti N. Ghia, and C. T. Shin. "High-Re solutions for incompressible flow using the Navier-Stokes equations and a multigrid method." *Journal of computational physics* 48, no. 3 (1982): 387-411. https://doi.org/10.1016/0021-9991(82)90058-4

[47] Kaazempur-Mofrad, M. R., S. Wada, J. G. Myers, and C. R. Ethier. "Mass transport and fluid flow in stenotic arteries: axisymmetric and asymmetric models." *International Journal of Heat and Mass Transfer* 48, no. 21-22 (2005): 4510-4517.https://doi.org/10.1016/j.ijheatmasstransfer.2005.05.004

[48] Hammoodi, Karrar A., Duaa Jassim Ayed, Muntadher H. Abed, Ammar Elsheikh, Mujtaba A. Flayyih, and As' ad Alizadeh. "Quantitative analysis of heat and mass transfer in MoS2-Al2O3/EG hybrid flow between parallel surfaces with suction/injection by numerical modeling of HPM method." *International Journal of Thermofluids* 24 (2024): 100819.https://doi.org/10.1016/j.ijft.2024.100819

[49] Eswari, A., L. Maragatham, N. Anbazhagan, Gyanendra Prasad Joshi, and Woong Cho. "Analytical Investigation of Heat and Mass Transfer in MHD Nano fluid Flow Past a Moving Vertical Plate." *Case Studies in Thermal Engineering* (2024): 104642.https://doi.org/10.1016/j.csite.2024.104642

[50] Bhogal, Sukhdeep, Cheng Zhang, Amer I. Aladin, Gary S. Mintz, and Ron Waksman. "Provisional versus dual stenting of left main coronary artery bifurcation lesions (from a comprehensive meta-analysis)." *The American Journal of Cardiology* 185 (2022): 10-17. https://doi.org/10.1016/j.amjcard.2022.09.012